Mechanical spectra of glass-forming liquids. II. Gigahertz-frequency longitudinal and shear acoustic dynamics in glycerol and DC704 studied by time-domain Brillouin scattering

Klieber, Christoph; Hecksher, Tina; Pezeril, Thomas; Torchinsky, Darius H.; Dyre, J. C.; Nelson, Keith Adam

Published in:
Journal of Chemical Physics

DOI:
10.1063/1.4789948

Publication date:
2013

Document Version
Publisher's PDF, also known as Version of record

Citation for published version (APA):
Klieber, C., Hecksher, T., Pezeril, T., Torchinsky, D. H., Dyre, J. C., & Nelson, K. A. (2013). Mechanical spectra of glass-forming liquids. II. Gigahertz-frequency longitudinal and shear acoustic dynamics in glycerol and DC704 studied by time-domain Brillouin scattering. *Journal of Chemical Physics*, *138*(12), 12A544 1-12. https://doi.org/10.1063/1.4789948

Mechanical spectra of glass-forming liquids. II. Gigahertz-frequency longitudinal and shear acoustic dynamics in glycerol and DC704 studied by time-domain Brillouin scattering

Christoph Klieber,[1,a)] Tina Hecksher,[2,b)] Thomas Pezeril,[3] Darius H. Torchinsky,[4] Jeppe C. Dyre,[2] and Keith A. Nelson[1,c)]
[1]*Department of Chemistry, Massachusetts Institute of Technology, Cambridge, Massachusetts 02139, USA*
[2]*DNRF Centre Glass and Time, IMFUFA, Department of Sciences, Roskilde University, DK-4000 Roskilde, Denmark*
[3]*Insitut Molécules et Matériaux du Mans, UMR CNRS 6283, Université du Maine, 72085 Le Mans, France*
[4]*Department of Physics, Massachusetts Institute of Technology, Cambridge, Massachusetts 02139, USA*

(Received 12 November 2012; accepted 17 January 2013; published online 26 February 2013)

This paper presents and discusses the temperature and frequency dependence of the longitudinal and shear viscoelastic response at MHz and GHz frequencies of the intermediate glass former glycerol and the fragile glass former tetramethyl-tetraphenyl-trisiloxane (DC704). Measurements were performed using the recently developed time-domain Brillouin scattering technique, in which acoustic waves are generated optically, propagated through nm thin liquid layers of different thicknesses, and detected optically after transmission into a transparent detection substrate. This allows for a determination of the frequency dependence of the speed of sound and the sound-wave attenuation. When the data are converted into mechanical moduli, a linear relationship between longitudinal and shear acoustic moduli is revealed, which is consistent with the generalized Cauchy relation. In glycerol, the temperature dependence of the shear acoustic relaxation time agrees well with literature data for dielectric measurements. In DC704, combining the new data with data from measurements obtained previously by piezo-ceramic transducers yields figures showing the longitudinal and shear sound velocities at frequencies from mHz to GHz over an extended range of temperatures. The shoving model's prediction for the relaxation time's temperature dependence is fairly well obeyed for both liquids as demonstrated from a plot with no adjustable parameters. Finally, we show that for both liquids the instantaneous shear modulus follows an exponential temperature dependence to a good approximation, as predicted by Granato's interstitialcy model. © *2013 American Institute of Physics*. [http://dx.doi.org/10.1063/1.4789948]

I. INTRODUCTION

The possibility of shear-wave propagation in liquids under specific conditions is well known.[1,2] At low frequencies, shear waves cannot propagate due to viscous damping, however at sufficiently high frequencies, any liquid becomes solidlike and allows for shear-wave propagation, although they are generally highly damped. The characteristic frequency separating the two regimes is given in terms of the Maxwell relaxation time τ_M as $1/\tau_M$, which we may represent in terms of the (DC) shear viscosity η and the instantaneous shear modulus G_∞ as $\tau_M = \eta/G_\infty$.[2] For ordinary low-viscosity liquids like ambient water, τ_M is on the order picoseconds, but for deeply supercooled liquids τ_M may be seconds, hours, or even longer.[3,4] At low frequencies ($\omega\tau_M \ll 1$), the shear stress is proportional to the shear rate. However, at high frequencies ($\omega\tau_M \gg 1$), the shear stress is proportional to the strain as for any solid.

When a liquid is cooled below its freezing temperature such that it avoids crystallization, its viscosity increases dramatically.[2,3,5] Consequently, the Maxwell relaxation time increases – roughly following the viscosity – and the characteristic frequency for onset of solidlike behavior decreases rapidly. The dynamics of the supercooled liquid state and of the glass transition, at which the liquid over a narrow temperature range falls out of equilibrium and freezes into a disordered solid, have been studied intensely for many years. In spite of these efforts, there is no agreement about what causes the dramatic slowing down, which in extreme cases can be as large as a factor of ten or more of the relaxation time for a temperature decrease of 1%. The most reliable data for the relaxation time's temperature dependence are from dielectric spectroscopy. There are only a handful of measurements on the mechanical properties of supercooled liquids (shear as well as longitudinal), which reflects the difficulty in obtaining data of suitable quality.[3] This is an important – indeed urgent – issue as mechanical properties define the constituting properties of liquids and solids, as well as the difference between these two phases of condensed matter.

On slow time scales, dynamic mechanical analysis,[6,7] and sonic or related measurement methods can be used to obtain data for a liquid's mechanical properties. Faster responses at MHz frequencies are accessible by ultrasonics[2] and impulsive stimulated thermal and Brillouin scattering (ISTS or ISBS, respectively).[8–12] Finally, the low GHz range may

a)Electronic mail: cklieber@mit.edu.
b)Electronic mail: tihe@ruc.dk.
c)Electronic mail: kanelson@mit.edu.

be accessed by spontaneous Brillouin scattering (BLS).[13] Recent work in x-ray Brillouin scattering has accessed THz longitudinal acoustic frequencies.[14,15] However, this technique is not yet capable of measurements of shear-acoustic dynamics in liquids. Deep-UV Brillouin scattering from longitudinal acoustic waves in this range has been demonstrated,[11,14] but is poorly adapted to measurements of shear relaxation in non-viscous liquids where the shear acoustic damping is always strong. Picosecond ultrasonics has provided tabletop access to most of the GHz frequency range for longitudinal acoustic waves.[16] In recent years, adaptations of this method to GHz shear wave generation through impulsive laser interaction have been developed.[17–27] Studies of shear waves in liquids, however, have remained elusive;[28] this is because it is generally much easier to monitor sound waves that are associated with local density variations than pure shear.

In recent articles,[29,30] we have demonstrated how a novel approach to time-domain Brillouin scattering (TDBS) using photo-acoustic generation and detection of frequency-tunable longitudinal and shear acoustic waves opens the window to the study of GHz frequency longitudinal and shear acoustic properties of liquids. We have demonstrated an experimental configuration that allows for measurements on viscous and non-viscous liquids alike. The present paper presents experimental results on the frequency- and temperature-dependent shear and longitudinal acoustic properties of glycerol ($C_3H_5(OH)_3$) and tetramethyl-tetraphenyl-trisiloxane, a silicone oil developed by Dow Corning under the trade name DC704, which is commonly used as diffusion pump fluid. In combination with results from other mechanical spectroscopic techniques, this provides a complete mechanical characterization of both liquids. Such characterizations are important by themselves, but also because they allow for tests of theories, for instance of the proposed connection between shear and longitudinal moduli (the generalized Cauchy relation[31]), or of the shoving model[5–7] connecting the non-Arrhenius temperature dependence of the relaxation time to the temperature dependence of the instantaneous shear modulus, G_∞.

Glycerol is a trihydric alcohol, an associated liquid that forms a weak hydrogen-bonding network and has a fragility index[32] of $m = 53$, making it intermediate between fragile and strong glass formers.[3,5,32] Glycerol is easily supercooled[33] below $T_m = 291$ K and forms a glass at $T_g \approx 186$ K. It is a prototypical and intensely studied glass former.[1,9,12,14,33–41] The wealth of available data for glycerol allows for a comparison of results obtained by different spectroscopic techniques. Unfortunately, glycerol easily absorbs water, which may result in poor reproducibility and should be kept in mind when comparing results from different laboratories. This is not a problem for the other liquid we studied, DC704, which is also a molecular glass former. DC704 has a glass transition temperature[34] of $T_g \approx 210$ K. The fragility index is $m = 95$,[42] making DC704 a typical fragile glass former. DC704 is entirely van der Waals bonded due to the presence of four phenyl groups: since oxygens are bonded to silicon, hydrogen bonding is absent in DC704. Moreover, the molecular dipole moment is quite small so dipole interactions are negligible. DC704 was also chosen because its dielectric and shear mechanical spectra do not show secondary relaxations at frequencies above the α relaxation[34] (often interpreted as a Johari-Goldstein or β_{slow}-relaxation). This simplifies the analysis of compiled spectra. Finally DC704, like glycerol, supercools easily and rarely crystallizes.

The first paper in this series presented low-frequency broadband bulk and shear mechanical spectra of two glass-forming liquids DC704 and 5-PPE obtained by the use of piezo-ceramic transducers.[43] The present paper is organized as follows. After a summary of the experimental technique in Sec. II, in Sec. III we present the results for the temperature dependence of the speeds of sound, acoustic attenuation coefficients, and moduli of glycerol and DC704 monitored at several fixed frequencies. Section IV examines the data within the context of two theories, the generalized Cauchy relation and the shoving model, and analyzes the temperature dependence of the instantaneous shear modulus. Section V concludes the paper with a brief summary.

II. EXPERIMENTAL TECHNIQUES

The recently developed TDBS technique[29] was used to investigate the frequency and temperature dependences of shear and longitudinal acoustic dynamics in liquids at GHz frequencies. A detailed description of this method was given in a separate publication;[30] in the following, we briefly summarize the most important aspects of the experimental approach, which combines different picosecond laser ultrasonic techniques for acoustic wave generation and detection.

Multiple-cycle longitudinal and shear acoustic waves were optically generated in a crystallographically canted metallic transducer film through the absorption of an optical pulse train,[44] where the subsequent rapid thermal expansion launched acoustic wave packets of both longitudinal and shear polarizations. The excitation pulses from a Ti:Sapphire amplifier system (Coherent RegA) operating at a 250 kHz repetition rate were centered around 790 nm with a bandwidth of about 8 nm and a pulse duration of 200 fs, and were focused on the sample to a 100 μm spot. Semitransparent transducer thin films were obliquely deposited under ultrahigh vacuum by molecular beam epitaxy[45] onto optical quality sapphire or BK7 glass substrates. The substrates consisted of monocrystalline columnar layers of iron with thicknesses between 40–50 nm and an average inclination angle of the iron grains of about 40°. The break of the shear symmetry in the direction normal to the sample ensured direct thermoelastic generation of shear acoustic plane waves,[22] in addition to longitudinal acoustic plane waves that do not require such a canted crystallographic orientation to be excited. After propagation into, and through, liquid layers with thicknesses ranging from single nanometers to several hundred nanometers, both shear and longitudinal acoustic waves were optically detected after transmission into a transparent substrate via TDBS.[16,46,47] The coherently scattered field, whose optical phase varied depending on the acoustic wave peak and null positions, superposed with the reflected probe field, resulting in signal intensity that showed time-dependent oscillations at the acoustic frequency.[48] This frequency ν was determined, as in any Brillouin scattering measurement, by the probe wavelength λ,

the scattering angle θ, the refractive index n, and the acoustic speed c in the substrate through

$$\nu = \frac{2\,n\,c}{\lambda}\,\sin\left(\frac{\theta}{2}\right).$$

In the present case, the probe was a frequency-doubled beam at 395 nm (focused to a 20 μm spot size), and either BK7 glass or sapphire was used for the detection substrate to provide access to lower and higher frequency ranges, respectively.

The detection of shear waves was optimal when the probe polarization and the shear acoustic wave polarization were both perpendicular to the plane of incidence. In this geometry, the interaction between the shear acoustic wave and the probe light resulted in a rotation of the polarization by 90° of the scattered light. The use of the combination of a half-wave plate (at 45°) and a polarizing cube beamsplitter assembly not only allowed to filter out common laser noise through balanced detection, but also allowed for optical heterodyning and provided sufficient sensitivity levels for the detection of extremely weak shear Brillouin signals.[30] Longitudinal wave detection did not pose any special requirements regarding the polarization of the detected probe light. The acoustic frequency that was excited may be varied by changing the excitation pulse sequence timing,[44] and this may be adjusted to match the longitudinal or shear Brillouin scattering frequency. In all cases, measurements were made at multiple lateral positions on the sample corresponding to multiple liquid layer thicknesses. A detailed description of the experimental configuration and the sample design can be found in Ref. 30. Differences in Brillouin signal amplitudes from acoustic waves that propagated through different liquid thicknesses yielded acoustic attenuation lengths. Differences in acoustic transit times across the liquid were observed as phase shifts in the time-dependent Brillouin signal oscillations and yielded the acoustic speed of the liquid.

Samples were prepared by squeezing the liquid under study between two optically clear substrates: a generation side substrate that held the iron generation transducer film and a curved or flat detection substrate. Anhydrous glycerol and DC704 were used as purchased from Sigma-Aldrich and forced through several linked 0.2 μm teflon millipore filters to remove dust particles before applying to the sample without further purification to eliminate water or gas contamination. The liquids were always stored under dry nitrogen atmosphere and the samples were made under dry nitrogen atmosphere after the sample substrate surfaces had been purged for 30 min to remove excess water and dust. After a sample was made, it was rapidly transferred to a cryostat and the sample chamber was immediately evacuated.

The approach described above that we used to determine the acoustic parameters of the liquids required the knowledge of the refractive index of both the liquid and the detection substrate (for the latter we used literature values and assumed no temperature dependence). The temperature-dependent refractive index (from T_g up to 400 K) for glycerol and DC704 at the optical detection wavelength of 395 nm was determined by means of a Michelson type interferometer. Out-gassed liquid was filled in a $l = 10$ mm cuvette, which was placed in the beam path of one interferometer arm inside a cryostat. One of the interferometer end mirrors was placed on a translation stage to allow for compensation of the temperature-dependent optical delay experienced by the light traveling through the liquid with respect to the same configuration for an empty cell.

The determined temperature dependence of the refractive index of glycerol can be well approximated by

$$n(T_g \le T \lesssim 400\,\mathrm{K}) = 1.680 - 6.5 \times 10^{-4}\,\mathrm{K}^{-1} \times T \quad (1)$$

and of DC704 by

$$n(T_g \le T \lesssim 400\,\mathrm{K}) = 1.750 - 4.9 \times 10^{-4}\,\mathrm{K}^{-1} \times T. \quad (2)$$

The determined temperature coefficient of the refractive index of DC704 is in excellent agreement with the temperature coefficient of 4.2×10^{-4} K^{-1} reported by Poulter and Nash[49] at 633 nm.

Furthermore, the calculation of the acoustic moduli required the knowledge of the temperature dependence of the mass density $\rho(T)$ for each liquid. The temperature dependence for glycerol above and below its glass transition temperature is given in Ref. 50 as

$$\rho(T < T_g) = 1\,390\,\tfrac{\mathrm{kg}}{\mathrm{m}^3} - 0.32\,\tfrac{\mathrm{kg}}{\mathrm{m}^3 K} \times T, \quad (3)$$

$$\rho(T > T_g) = 1\,450\,\tfrac{\mathrm{kg}}{\mathrm{m}^3} - 0.66\,\tfrac{\mathrm{kg}}{\mathrm{m}^3 K} \times T. \quad (4)$$

For DC704, we deduce the following expression for the temperature dependence of the density by assuming a constant expansion coefficient α_p at temperatures above T_g,

$$\rho(T > T_g) = \frac{1\,070\,\mathrm{kg\,m^{-3}}}{1 + 7.2 \times 10^{-4}\,\mathrm{K}^{-1} \times (T - 298\,\mathrm{K})}, \quad (5)$$

where the value used $\alpha_p(T = 298\mathrm{K}) = 7.2 \times 10^{-4}\,\mathrm{K}^{-1}$ was given by Orcutt.[51]

III. TEMPERATURE DEPENDENCE OF ACOUSTIC PARAMETERS AT FIXED FREQUENCIES

In this section, we present the experimental results for the temperature-dependent measurements of the speed of sound and attenuation coefficient in glycerol and DC704 at a fixed detection frequency of $\nu_S = 25$ GHz for shear waves and $\nu_L = 41.5$ GHz for longitudinal waves. We present these data alongside data from a large range of frequencies obtained by other techniques.

The mechanical response (longitudinal or shear) of a material at a given temperature T and frequency ν is usually expressed either in terms of a complex modulus $\hat{C}(T, \nu)$ or in terms of a speed of sound $c(T, \nu)$ (defined as the phase velocity of the acoustic wave) and the corresponding attenuation coefficient $\alpha(T, \nu)$. The two representations are equivalent and mathematically connected via the temperature-dependent density $\rho(T)$ and the *complex* acoustic velocity $\hat{c}(T, \nu)$ via

$$\hat{C}(T, \nu) = \rho(T)\,\hat{c}(T, \nu)^2\,. \quad (6)$$

In our measurements, the complex acoustic velocity is defined by $\hat{c} = 2\pi\nu/\hat{q}$, where $\hat{q}$ is the complex wavevector

TABLE I. Temperature dependent longitudinal and shear speeds of sound and attenuation coefficients for glycerol recorded by TDBS in a BK7 detection substrate with no prism. The Brillouin scattering frequencies are 41.5 GHz and 25.0 GHz for longitudinal and shear acoustic waves, respectively. Results are plotted in Figs. 1(a) and 1(b).

T [K]	c_L [ms^{-1}]	α_L [10^{6}m^{-1}]	c_S [ms^{-1}]	α_S [10^{6}m^{-1}]
180	3630 ± 60	0.18 ± 0.04	1930 ± 50	0.84 ± 0.24
190	3610 ± 60	0.22 ± 0.04	1910 ± 50	0.96 ± 0.24
200	3560 ± 60	0.25 ± 0.07	1850 ± 50	1.2 ± 0.2
210	3530 ± 70	0.34 ± 0.07	1800 ± 50	1.8 ± 0.5
220	3460 ± 60	0.42 ± 0.12	1740 ± 70	2.3 ± 1.0
235	3380 ± 50	0.69 ± 0.18	1650 ± 50	3.6 ± 1.2
250	3300 ± 50	1.1 ± 0.2	1560 ± 50	6.0 ± 2.4
265	3170 ± 70	1.8 ± 0.4	1470 ± 70	9.6 ± 3.6
280	3080 ± 60	2.8 ± 0.6	1370 ± 70	13 ± 5
295	2930 ± 50	5.0 ± 1.0	1250 ± 50	20 ± 7
310	2830 ± 60	7.2 ± 1.8	1160 ± 50	24 ± 8
325	2730 ± 70	9.6 ± 2.0	1030 ± 50	30 ± 8

$\hat{q} = 2\pi\nu/c + i\,\alpha$. We note that the real part of the complex acoustic velocity defined this way is *not* identical to the speed of sound, Re $\{\hat{c}\} \neq c$, except at low attenuation, i.e., for $\alpha \to 0$. For longitudinal acoustic parameters, the relevant modulus is the longitudinal modulus $\hat{M} = M' + i\,M'' = \rho\,\hat{c}_L^2$, and for transverse acoustic parameters it is the shear modulus $\hat{G} = G' + i\,G'' = \rho\,\hat{c}_S^2$ (here the subscripts L and S denote longitudinal and shear, respectively). These two different representations should be kept in mind by the reader and are used interchangeably below.

A. Glycerol

Results obtained by TDBS for glycerol are listed in Table I and displayed in Fig. 1 together with data obtained from frequency-domain Brillouin scattering measurements at similar frequencies (~20 GHz from Ref. 39). In the case of longitudinal waves, TDBS and frequency-domain Brillouin scattering show excellent agreement, indicating that there is little dispersion over this frequency and temperature range except for the highest reported temperatures, where the two measurements separate. As expected, the lower probe frequency is sensitive to the structural relaxation at a lower temperature than the higher probe frequency.

We recall that the Maxwell relaxation time is defined by $\tau_M = \eta_S/G_\infty$. Identifying τ_M with the average relaxation time $\langle\tau_\alpha\rangle$, we can estimate the shear viscosity η_S from our measured values for G_∞ and from literature values for the average relaxation time in glycerol. Figure 2 compares values of the shear viscosity calculated by multiplying G_∞ by the relaxation times $\langle\tau_\alpha\rangle$ as measured by dielectric spectroscopy from Ref. 52 with static shear viscosity data measured by Schroter *et al.*[35] The two data sets have very similar temperature dependences, but differ by approximately a factor of 2. This is not surprising, given that average relaxation times obtained from different techniques are not required by theory to be identical. Below the viscosity plot of Fig. 2, we show the timescale index, defined as the ratio of the measured and calculated shear viscosity. Significant deviations from experimentally measured values of η_S (or equivalently: a large and temperature-dependent timescale index) are typical for systems with secondary relaxation or weak translational-rotational coupling.[53] The investigation of translational-rotational coupling in glycerol is difficult due to its small Brillouin cross-section and polarizability anisotropy. Our results indicate, however, that the coupling is relatively strong and independent of temperature. Evidently, the

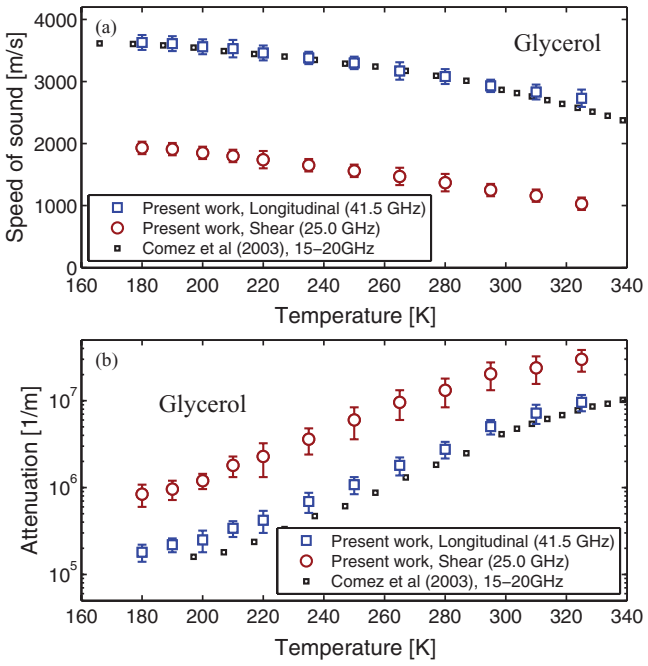

FIG. 1. (a) Results for the temperature dependent longitudinal (41.5 GHz) and shear (25 GHz) acoustic speeds and (b) attenuation coefficients of glycerol from T_g up to 325 K. Literature data for the longitudinal sound velocity and attenuation rate as measured by polarized frequency-domain Brillouin scattering measurements (in the VV geometry) at similar frequencies are from Ref. 39. The onset of longitudinal acoustic dispersion can be seen in (a) for the two illustrated frequencies at temperatures above 300 K.

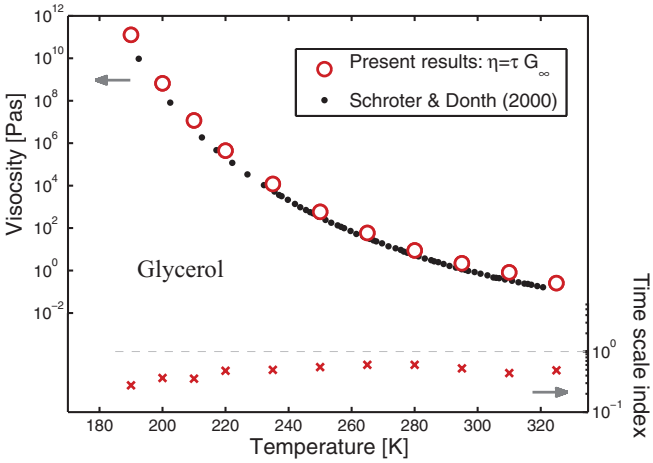

FIG. 2. Temperature dependence of the shear viscosity. Circles are calculated by the relationship $\eta_S = G_\infty\langle\tau_\alpha\rangle$, where the values of G_∞ come from the present work and $\langle\tau_\alpha\rangle$ are dielectric relaxation times taken from Ref. 52. Dots represent the measured shear viscosity from Ref. 35. Below, the time scale index, i.e., $\eta_{\text{measured}}/\eta_{\text{calculated}}$, is shown. The time scale index is small (~0.5) and only weakly temperature dependent.

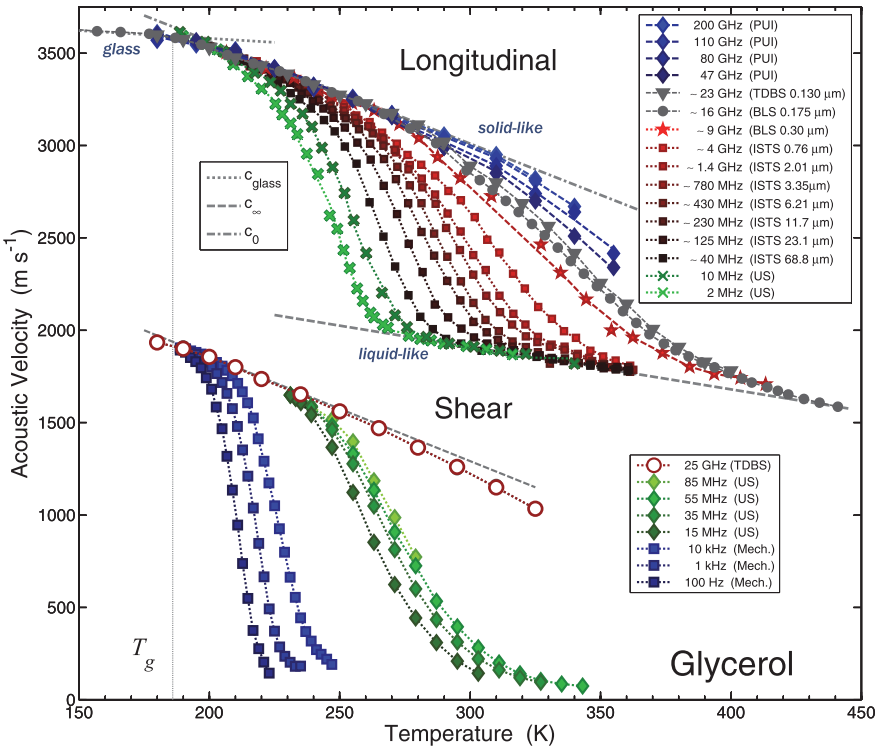

FIG. 3. Combined longitudinal and shear speeds of sound in glycerol at a wide range of frequencies as a function of temperature. Longitudinal speeds are taken from the following sources: PUI from Ref. 59 and time-domain Brillouin scattering (TDBS) from Ref. 30, Brillouin light scattering (BLS) at wavevectors $\lambda = 0.175\ \mu$m from Ref. 39 and $\lambda = 0.30\ \mu$m from Ref. 13, impulsive stimulated thermal scattering (ISTS) from Ref. 8, and US from Ref. 60. Present results from TDBS shear measurements are shown together with results from conventional ultrasonics from Ref. 1, and mechanical measurements (Mech) from Ref. 61.

dielectric – roughly equivalent to the rotational – relaxation time is slower than the Maxwell – roughly equivalent to the translational – relaxation time. Similar observations, slower rotational relaxation time and constant decoupling index, were reported by Dreyfus *et al.*[53] for *m*-toluidine and more recently by Torchinsky *et al.*[54] for triphenylphosphite and Jakobsen *et al.*[55] for two other glass-forming liquids. Glycerol, however, is not a strongly correlating liquid,[56–58] and for this reason there are no theoretical arguments for the absence of a relaxation time decoupling.

The temperature dependences of both the longitudinal and shear speeds of sound in glycerol are shown in Fig. 3 supplemented by results from a variety of different techniques. Together these techniques cover frequencies from 100 Hz up to several hundreds of GHz.

The highest frequencies for the longitudinal data are obtained using picosecond ultrasonic interferometry (PUI)[59] and time-domain Brillouin scattering (TDBS).[59] The spontaneous BLS results are from Comez *et al.*[39] (at wavelength $\lambda = 0.175\ \mu$m) and Pinnow *et al.*[13] (at wavelength $\lambda = 0.3\ \mu$m), corresponding to frequencies in the low GHz region. Impulsive stimulated thermal scattering from Ref. 8 covers most of the MHz region. Finally, the lowest MHz frequencies (2 and 10 MHz) were measured by Jeong *et al.*[60] by conventional ultrasonic techniques. There is excellent agreement between the results from all techniques.

The present results for the shear speed of sound represent the highest available frequency at 25 GHz. Megahertz data (between 15 MHz and 85 MHz) were obtained by Piccarelli and Litovitz using a standard ultrasonic (US) transducer technique.[1] Because of the high attenuation, acoustic velocities and attenuation could not be measured directly. Instead the real and imaginary parts of the shear impedance, $\rho c'_S$ and $\rho c''_S$, were measured. Results were reported in terms of ${\rho c'_S}^2$ and G', from which we can calculate the shear speed of sound. Low-frequency shear measurements at 100 Hz, 1 kHz, and 10 kHz were made by Jeong[61] using a piezoelectric transducer technique. Data were reported in terms of the real and imaginary parts of the shear modulus, unfortunately however, only in normalized – not absolute – values. The data were adjusted to match our measurements and the depolarized BLS data of the real shear modulus close to the glass transition temperature, where G' is not expected to have any frequency dependence. The results from the different techniques show excellent agreement.

For longitudinal waves, both low and high frequency limits of the speed of sound are finite. The former gives the "liquid-like" adiabatic sound velocity $c_{L,0}$, while the latter gives the "solid-like" velocity of sound $c_{L,\infty}$, i.e., the high-frequency limit where the period of the wave is shorter than the structural relaxation time τ_α. The zero-frequency limit of the longitudinal sound speed from all different techniques between 270 K and 440 K may be approximated by the following expression:

$$c_{L,0} = (2610 \pm 5)\ \tfrac{\mathrm{m}}{\mathrm{s}} - (2.3 \pm 0.02)\ \tfrac{\mathrm{m}}{\mathrm{sK}} \times T, \qquad (7)$$

which is in excellent agreement with reported values by Comez *et al.*[39] for their temperature range between 307 K and 390 K. Similarly, a fit of the speed of sound vs. temperature yields an expression for the solidlike longitudinal sound speed

$$c_{L,\infty} = (4640 \pm 10)\,\tfrac{\mathrm{m}}{\mathrm{s}} - (5.5 \pm 0.5)\,\tfrac{\mathrm{m}}{\mathrm{sK}} \times T. \qquad (8)$$

For the shear speed of sound there is only an upper finite bound, $c_{S,\infty}$, reflecting the fact that shear acoustic waves do not propagate at frequencies that are low compared with the inverse structural relaxation time (the shear modulus vanishes at low frequencies). A linear fit of the instantaneous shear sound velocity as a function of temperature yields

$$c_{S,\infty} = (2990 \pm 30)\,\tfrac{\mathrm{m}}{\mathrm{s}} - (5.7 \pm 0.1)\,\tfrac{\mathrm{m}}{\mathrm{sK}} \times T. \qquad (9)$$

Figure 3 also shows that the slope of the solidlike behavior changes at the glass-transition temperature. It is sometimes an overlooked fact that the infinite-frequency sound speeds of the equilibrium liquid and of the glass are not identical; in fact, these quantities are not only different, but have temperature dependencies that are quite different. This is easy to understand intuitively if one naively imagines a model in which the high-frequency sound velocities are functions of density, in which case the different expansion coefficients of the liquid and the glass must result in these differences; however, there are only a few examples in the literature that document this difference experimentally.[38,83]

B. DC704

The second liquid under study was the silicone oil tetramethyl-tetraphenyl-trisiloxane (DC704). The obtained longitudinal and shear speeds of sound and attenuation coefficients at temperatures between 200 K and 300 K are listed in Table II and displayed in Fig. 4. In this measurement, acoustic waves were generated in an iron transducer film on a sapphire substrate and detected in a 2.5 cm BK7 substrate.

Since the measurement technique used in the present work, briefly described in Sec. II, does not depend on the material's acousto-optical properties (as is the case for impulsive stimulated scattering and conventional BLS measurements), our somewhat poorer data quality for DC704 compared with that of glycerol can be explained by the mechanical properties of the liquid. The main consideration is the significantly lower acoustic transmission coefficient of the acoustic wave both from the transducer into the liquid and from the liquid into the detection material. In order to better understand this point, we examine the acoustic transmission coefficient T_a from one material ($i = 1$) into another material ($i = 2$). This quantity is defined as $T_a = (2\,Z_1\,Z_2/(Z_1 + Z_2))^2$, where $Z_i = \rho_i\,c_i$ is the acoustic impedance of the material i. From this equation, we directly see that transmission between materials with large differences in acoustic impedance becomes small (i.e., there is poor impedance matching). In our case, the acoustic impedance of both transducer film and detection substrate are larger than that of either liquid under study. But the acoustic impedance of DC704 is about half of that of glycerol, and therefore the overall acoustic transmission of the generated pulse train from the transducer into the detection substrate is significantly reduced. In addition, by comparing Fig. 1(b) with Fig. 4(b) we see that the acoustic attenuation of DC704 is about a factor of five to ten times larger than that of glycerol at the glass transition which further decreases the signal/noise of the measurements.

Figure 5 shows the temperature dependence of the longitudinal and shear speeds of sound in DC704 at different frequencies compiled from different measurement techniques. The present results represent the highest frequencies reported for both the longitudinal and the shear data, at 41 GHz and 25 GHz, respectively. Results from TDBS measurements at the two probe lengths 395 nm and 790 nm directly in the

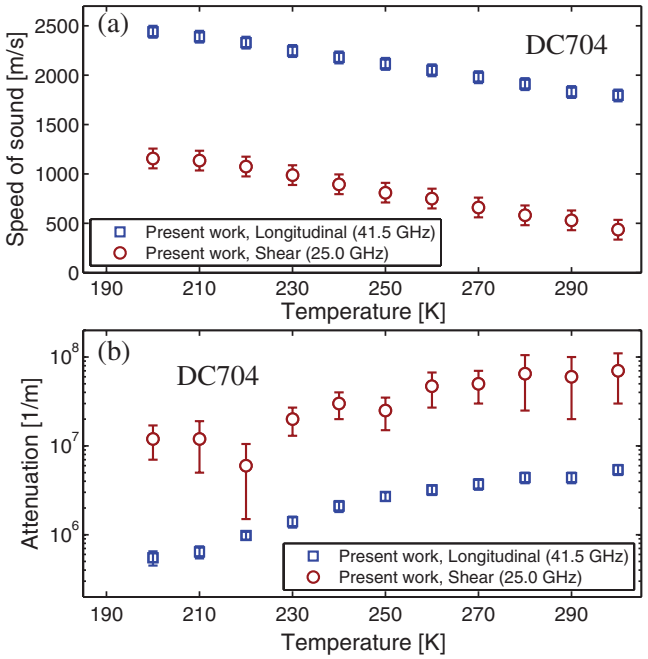

FIG. 4. Temperature dependent longitudinal and shear speeds of sound and attenuation coefficients of DC704 (a) and (b). The Brillouin scattering frequencies for longitudinal waves (41.5 GHz) and for shear waves (25.0 GHz) were defined by the BK7 glass detection substrate and the probe light scattering angle in the detection substrate of ∼30°.

TABLE II. Same sample and detection configuration as used for the measurements of Table I but for the liquid DC704. Results are plotted in Fig. 4. Longitudinal and transverse frequencies were 41.0 and 25.0 GHz.

T [K]	c_L [ms^{-1}]	α_L [10^6 m^{-1}]	c_S [ms^{-1}]	α_S [10^6 m^{-1}]
200	2440 ± 30	0.55 ± 0.10	1156 ± 50	12 ± 5
210	2390 ± 30	0.64 ± 0.10	1135 ± 50	12 ± 7
220	2330 ± 30	0.98 ± 0.10	1075 ± 50	6.0 ± 4.5
230	2245 ± 30	1.4 ± 0.2	988 ± 50	20 ± 7
240	2180 ± 30	2.1 ± 0.3	895 ± 50	30 ± 10
250	2115 ± 30	2.7 ± 0.3	810 ± 50	25 ± 10
260	2050 ± 30	3.2 ± 0.4	750 ± 50	47 ± 20
270	1980 ± 30	3.7 ± 0.5	660 ± 50	50 ± 20
280	1910 ± 30	4.4 ± 0.6	580 ± 50	65 ± 40
290	1830 ± 30	4.4 ± 0.6	530 ± 50	60 ± 40
300	1795 ± 30	5.4 ± 0.7	435 ± 50	70 ± 40

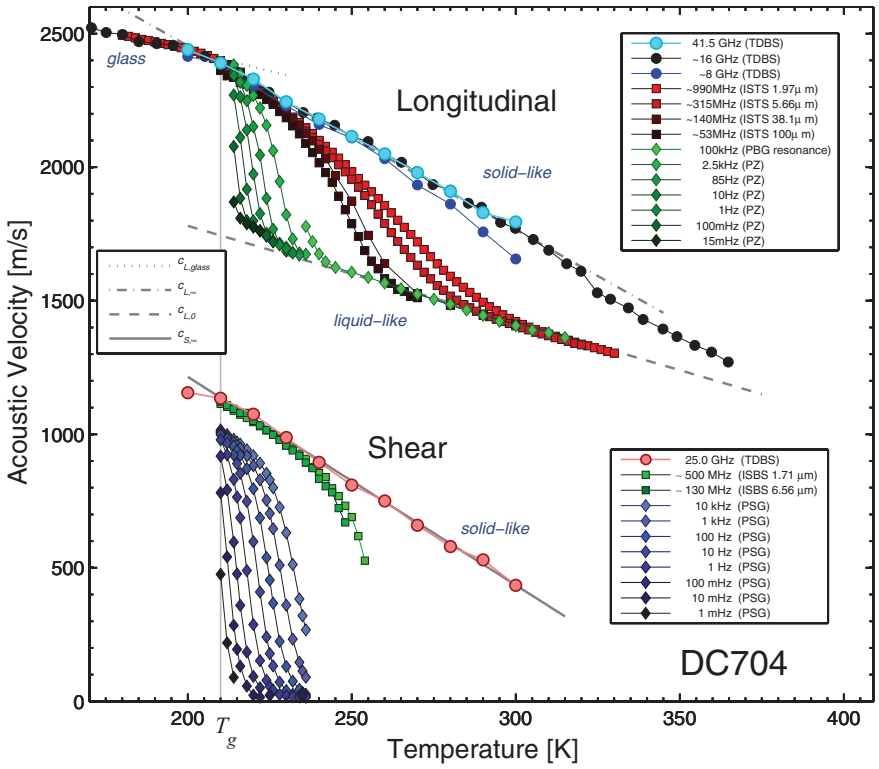

FIG. 5. Combined longitudinal and shear speeds of sound in DC704 at a wide range of frequencies as a function of temperature. Longitudinal speeds of sound were obtained by the following techniques: Time-domain Brillouin scattering (TDBS) from the substrate as well as measured directly in the liquid at two fixed wavevectors, impulsive stimulated thermal scattering (ISTS),[62] and piezo-electric modulus gauge techniques (PZ).[43] Shear speeds of sound from TDBS shear measurements (present results) are shown together with results from impulsive stimulated Brillouin scattering (ISBS) and the piezoelectric shear modulus gauge technique (PSG). Details on the ISTS/ISBS techniques can be found in Refs. 63 and 64. For details (and further references) on the PZ/PSG techniques, Paper I of the series[43] can be consulted.

liquid give the longitudinal speed of sound at roughly 8 GHz and 16 GHz, while most of the MHz region was covered by the ISTS technique. The piezoelectric modulus gauge (PZ) techniques covers frequencies from ∼10 mHz to ∼100 kHz (see Paper I for details).

The shear speed of sound was measured by ISBS at two wavelengths, corresponding to approximately 130 and 500 MHz frequencies, and by the PSG at frequencies from 1 mHz to 10 kHz (we refer the reader to Paper I for details of the PSG technique).

The agreement between the various techniques is good, although there is a ∼10% discrepancy on the limiting shear sound velocity, $c_{s,\infty}$, as measured by the high and low frequency techniques. This reflects a systematic error in the calibration between the piezo-ceramic methods and the present results.

The data for DC704 exhibit all the well-known features expected of the structural relaxation process of a viscous liquid: a marked dispersion of the speed of sound, a typical S-shape dispersion curve that is bounded by the limiting high and low frequency values of the velocity, and a change in the slope in $c_\infty(T)$ at about 210 K reflecting the liquid-glass transition.

The large frequency range made available by piecing together data obtained by various techniques enables us to give approximate expressions for both the low- and high-frequency limiting sound velocities over a broad range of temperatures. Data obtained from different techniques were fitted in the region from 220 K to 350 K yielding the following expression for the zero-frequency (liquid-like) longitudinal sound velocity $c_{L,0}$:

$$c_{L,0} = (2470 \pm 10)\,\tfrac{\mathrm{m}}{\mathrm{s}} - (3.52 \pm 0.02)\,\tfrac{\mathrm{m}}{\mathrm{sK}} \times T. \qquad (10)$$

At frequencies high compared to the inverse alpha relaxation time, the speed of sound again becomes independent of frequency and depends solely on the temperature. The temperature dependence of the infinite-frequency (solid-like) longitudinal speed of sound may also be approximated by a linear expression

$$c_{L,\infty} = (3840 \pm 10)\,\tfrac{\mathrm{m}}{\mathrm{s}} - (6.9 \pm 0.4)\,\tfrac{\mathrm{m}}{\mathrm{sK}} \times T. \qquad (11)$$

Close to the glass transition of DC704 at $T_g = 210$ K, we observe the aforementioned expected crossover to another approximately linear behavior, as follows:

$$c_{L,\mathrm{glass}} = (3040 \pm 10)\,\tfrac{\mathrm{m}}{\mathrm{s}} - (3.05 \pm 0.04)\,\tfrac{\mathrm{m}}{\mathrm{sK}} \times T. \qquad (12)$$

Finally, a linear fit of the infinite-frequency shear sound velocity yields

$$c_{S,\infty} = (2780 \pm 50)\,\tfrac{\mathrm{m}}{\mathrm{s}} - (7.8 \pm 0.2)\,\tfrac{\mathrm{m}}{\mathrm{sK}} \times T. \qquad (13)$$

From the fits of the high-frequency limits of the liquid and glassy states, Eqs. (11) and (12), it is possible to

determine the crossover temperature to be 208 ± 5 K. This is identical to the definition of the glass transition temperature as defined through $\tau(T_g) = 100$ s within the experimental uncertainty.

IV. COMPARING TO THE GENERALIZED CAUCHY RELATION AND THE SHOVING MODEL PREDICTION

When atoms in a crystalline material interact via a central potential, the Cauchy identity[65] holds. The Cauchy identity, which reduces the number of independent elastic moduli in an isotropic system from two to one, states that the longitudinal modulus M is related to the shear modulus G by $M = 3G$. Although liquids are isotropic, this relation cannot hold in general for liquids, where the moduli are complex and frequency dependent, because G goes to zero at low frequencies, whereas M converges to a finite value in the same limit. One way to extend the Cauchy identity to liquids is to assume that it holds merely for the high-frequency (instantaneous) moduli, $M_\infty = 3G_\infty$. This identity, however, rarely holds in experiment.[31] After noting this Krüger *et al.*[31] suggested a generalized Cauchy-like relation of the form

$$M_\infty = A + BG_\infty, \tag{14}$$

where A and B are system-dependent, temperature-independent constants. This was found to hold across a wide temperature range down to the glass transition temperatures of different liquids. Typical values of B are found to be close to 3 in a number of different glass-formers, including organic and inorganic glasses, as well as some bulk metallic glasses.[31,66,67] We find below, however, somewhat smaller B values.

The modified Cauchy relation (Eq. (14)) can be tested readily by comparison of the temperature evolution of the elastic moduli, M_∞ and G_∞ from Fig. 6(a). The results for glycerol are presented in Fig. 6(b) and a linear fit gives $A = (6.5 \pm 0.6)$ GPa and $B = (2.3 \pm 0.1)$ as best-fit parameters. We included all available points although there are signs of dispersion at some of the higher temperatures.

Even though the temperature range of our DC704 data is smaller than that of glycerol, the same analysis in terms of a modified Cauchy relation can be carried out for DC704. Figure 7(a) shows the real parts of our longitudinal and shear acoustic modulus data as calculated from the speeds of sound, the acoustic attenuation coefficients (both shown in Fig. 4) and the temperature dependence of the density as given by Eq. (5). In Fig. 7(b), we plot the instantaneous shear modulus G_∞ against the instantaneous longitudinal modulus M_∞. A linear fit to the data is possible within the experimental uncertainties, giving $A = (3.2 \pm 0.5)$ GPa and $B = (2.4 \pm 0.4)$ as best-fit parameters.

It was proposed some time ago that the instantaneous shear modulus G_∞ controls the fragility as the activation energy is controlled by the energy cost associated with a non-compressional rearrangement of molecules by pushing aside their neighbors.[6,68] This "shoving" model views collective relaxation as a series of individual relaxation events that take the system between configurational minima. This perspective recalls landscape-activated models[69,70] for the glass transition, and in recent years has been equated with them.[71,72] The shoving model predicts that the temperature dependence of the activation energy arises solely from that of the instantaneous shear modulus G_∞. This result is arrived at via the core assumptions that the average relaxation time is dictated only by flow and that during a flow event, the molecules do not rearrange at constant volume. The model argues that this is the case, because the energy cost from rearranging at constant volume arising from the strongly anharmonic repulsive piece of the intermolecular potential is prohibitively high. Rather, it is more energetically favorable for a molecular rearrangement to take place by a local expansion whereby the molecules perform work on their neighbors. This work constitutes the main energy barrier to be overcome.[68] In analyzing the nature of this work, one first assumes that the molecular displacements are purely radial. In this case, perhaps counterintuitively, no compressional work is done on the surrounding medium; rather than a change in density, the neighboring molecules are simply "shoved" aside during flow (with a radial displacement field varying with distance from the flow event as $1/r^2$). With no change in density, the energy required is due exclusively to the contribution from the shear elastic modulus. As these motions take place at very short time scales, the relevant quantity is the instantaneous shear modulus.

In the framework of the shoving model, a relaxation event is considered as an activated process. The average relaxation time τ depends on temperature as $\tau \sim \exp(\Delta E_r(T)/k_B T)$,

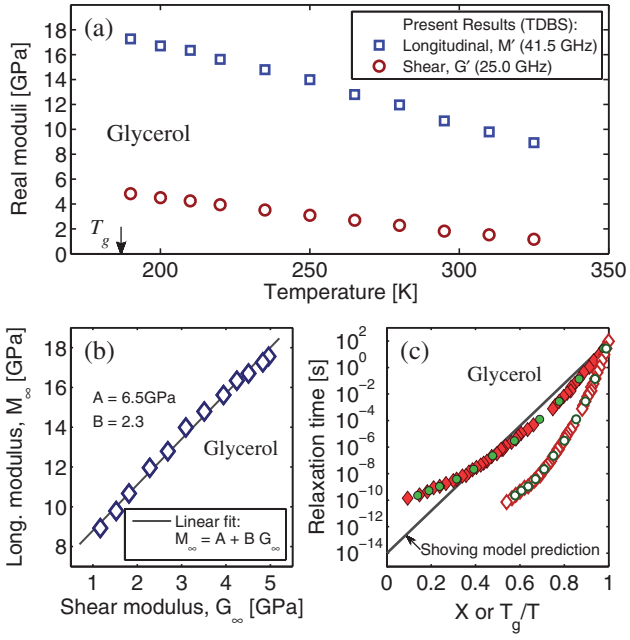

FIG. 6. (a) Real parts of the longitudinal and shear acoustic moduli of glycerol (same data as Fig. 1(a) omitting temperatures below T_g). (b) Linear fit to the longitudinal elastic modulus plotted vs. the shear elastic modulus. (c) Test of the shoving model (Eq. (15)) linear relationship between $X = (G_\infty(T)\,T_g)/(G_\infty(T_g)\,T)$ and relaxation time (Eq. (17)). The plot shows the relaxation time (from Ref. 52) as a function of normalized inverse temperature T_g/T (open symbols) and as a function of X (closed symbols), as well as the model prediction (straight line). Circles represent interpolation of relaxation time data at temperatures where G_∞ was measured, diamonds represent interpolation of the G_∞ values at temperatures where relaxation time was measured.

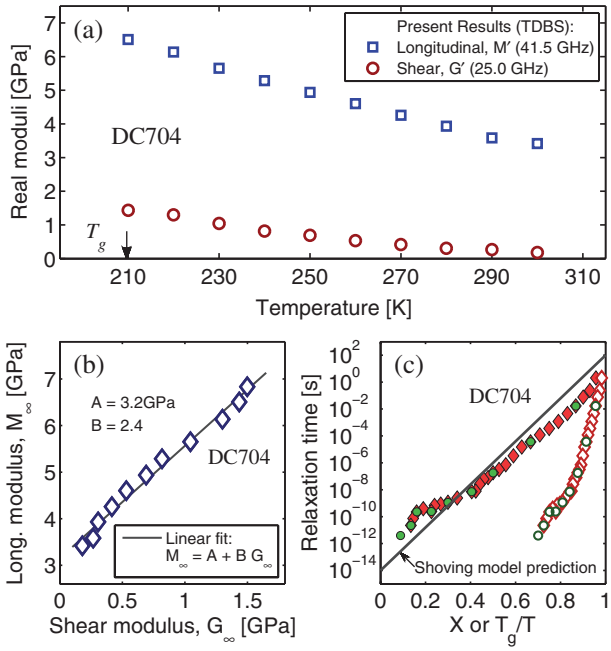

FIG. 7. (a) Real parts of the longitudinal and shear acoustic moduli of glycerol (same data as Fig. 4(a), except temperatures below T_g are excluded). (b) Linear fit to the longitudinal elastic modulus plotted vs. the shear elastic modulus. (c) Test of the shoving model (Eq. (15)) of linear relationship between $X = (G_\infty(T)\,T_g)/(G_\infty(T_g)\,T)$ and relaxation time (Eq. (17)). The relaxation time (from Ref. 62) is plotted as a function of T_g/T (open symbols) and as a function of X (closed symbols). Circles represent interpolation of relaxation time data at temperatures where G_∞ was measured, diamonds represent interpolation of G_∞ at temperatures where relaxation time was measured.

where the activation energy ΔE_r is temperature dependent. Its temperature dependence derives exclusively from that of the instantaneous shear modulus G_∞. Thus, the average relaxation time is given as

$$\tau(T) = \tau_0 \exp\left(\frac{G_\infty(T) V_c}{k_B T}\right). \tag{15}$$

Here, τ_0 is a high-temperature limit of the relaxation time, typically on the order of picoseconds, and V_c is a "characteristic" volume associated with the flow event (given by $V_c = 2/3 \cdot \Delta V^2/V$, where ΔV is the change in volume during the flow event and V is the volume of the flowing region before the flow event). In practice, it is impossible to estimate the value of V_c and in order to limit the number of fitting parameters, the shoving model simply assumes V_c is temperature independent.

In order to compare to experimental data, it is convenient to introduce the coordinate X provided by examining the logarithm of the characteristic relaxation time τ versus the normalized right-hand side of Eq. (15),

$$X = \frac{G_\infty(T) T g}{G_\infty(T_g) T}. \tag{16}$$

The variable X runs from zero in the high-temperature liquid state to unity at T_g, for which we have used the standard definition that T_g is the temperature at which the equilibrated liquid's relaxation time is 100 s. In the high-temperature liquid state limit, we take τ to represent an inverse attempt frequency (which is more or less a microscopic vibration time), so here we have fixed the value to $\tau_0 = 10^{-14}$ s. With these parameters the shoving model prediction is

$$\log(\tau) = 16X - 14. \tag{17}$$

A test of the shoving model (Eq. (15)) requires investigating the correlation of X as described by Eq. (16) with the relaxation time at the same temperature as deduced, e.g., from viscosity data via the Maxwell relation, or the relaxation times determined from shear or dielectric relaxation. For the analysis of glycerol, we used the dielectric relaxation times reported by Lunkenheimer *et al.*[52] Figure 6(c) shows the relaxation times as a function of normalized inverse temperature T_g/T (open symbols) as well as of the variable X (closed symbols). A similar comparison is shown for DC704 in Fig. 7(c) where the relaxation times are taken from the broadband study of the longitudinal modulus.[62] For both glycerol and DC704, we used spline interpolation to obtain relaxation times at the precise temperatures where G_∞ was measured (circles) as well as G_∞ at the temperatures where relaxation time data were available (diamonds). As expected, it does not matter which property is interpolated. The plot of relaxation times versus X does not give completely the predicted line in either case. At high temperatures we note the presence of an inflection, which could be due to the liquid becoming dispersive even at the high measuring frequency (25 GHz). Although the shoving model is not expected to apply when flow events are no longer thermally activated at high temperatures, this inflection is somewhat puzzling given that the relaxation time should converge to the prefactor value as $T \to \infty$. Overall, however, we conclude that the shoving model gives a qualitatively good description of the non-Arrhenius temperature dependence of the relaxation time for both liquids.

We note that under the above assumptions an estimate of V_c can be provided as $V_c = 16 k_B T_g / G_\infty(T_g)$. Plugging in the values for glycerol and DC704, we find $V_c^{\text{glycerol}} = 8.5 \times 10^{-30}$ m^3 and $V_c^{\text{DC704}} = 3.1 \times 10^{-29}$ m^3 corresponding to a length scale ($\propto V_c^{1/3}$) of 2 Å and 3 Å respectively, or roughly the size of the molecule, which is reasonable.

A. Temperature dependence of the instantaneous shear modulus

In Secs. III A and III B, we have assumed a linear temperature dependence of the infinite-frequency shear speed of sound (Eqs. (9) and (13)). Looking at Figs. 6(a) and 7(a), a linear fit $G_\infty(T)$ would be just as suitable. However, both these functional forms cannot be correct since $G_\infty = \rho c_{S,\infty}^2$. Moreover, at high temperatures both expressions will eventually fail when the extrapolated G_∞ either becomes negative or starts to grow after a minimum. The interstitialcy model of Granato[73,74] operates with an exponential temperature dependence,

$$G_\infty(T) = b \exp(-aT). \tag{18}$$

In Fig. 8, we compare these three functional forms of the instantaneous shear modulus to data. We show in this figure the real part of the shear modulus of glycerol and DC704 (open circles) both on a linear and on a logarithmic scale for

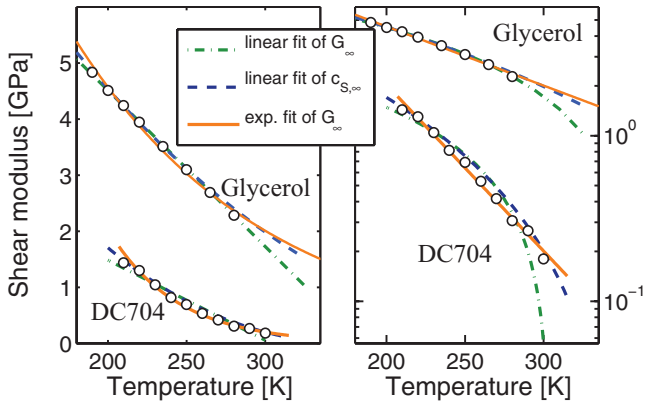

FIG. 8. Functional form of the temperature dependence of the instantaneous shear modulus. Real part of the shear modulus (G_∞) of glycerol and DC704 and various functional forms: linear fit of $G_\infty(T)$, linear fit of $c_{S,\infty}$, and exponential fit of $G_\infty(T)$. Data and fits are plotted both linearly (left) and logarithmically (right) as a function of temperature.

temperatures where the dynamics are non-dispersive, i.e., where G'' is small and we can assume $G' = G_\infty$. The figure also shows the linear fit to $G_\infty(T)$ (dashed-dotted line), $G_\infty(T)$ based a linear fit to $c_{S,\infty}(T)$ using Eq. (6) ($\hat{G} = \rho\hat{c}_S^2$) in the $\omega \to \infty$ limit (dashed line) and an exponential fit to $G_\infty(T)$ (full line). For glycerol, the three functional forms do not give noticeably different fits to data (the linear fit to G_∞ being slightly more convincing), but for DC704 the exponential fit is superior.

Note that when the data sets for both liquids are plotted together, it becomes apparent that there is a large difference in the absolute values of the instantaneous shear modulus of the two liquids, glycerol being roughly four times more rigid than DC704.

Figure 9(a) shows the relaxation time as a function of inverse temperature multiplied by $G_\infty(T)$. Figure 9(b) shows the relaxation time as a function of inverse temperature and the "calculated" relaxation times using Eq. (15), the measured $G_\infty(T)$, and the best fitted values of V_c and τ_0, as well as the predicted curve using the three different fits of $G_\infty(T)$ presented in Fig. 8. For glycerol, the choice of functional form does not make any significant difference; none of the curves capture the shape of temperature dependence of the relaxation time convincingly, although the exponential fit is slightly better. For glycerol it seems that the temperature dependence of G_∞ is not quite strong enough to account for the super-Arrhenius behavior. For DC704, on the other hand, the different fits of G_∞ result in quite different models for relaxation time. Here, the exponential fit follows accurately the data over a large temperature region, while the two alternative fits do a poorer job.

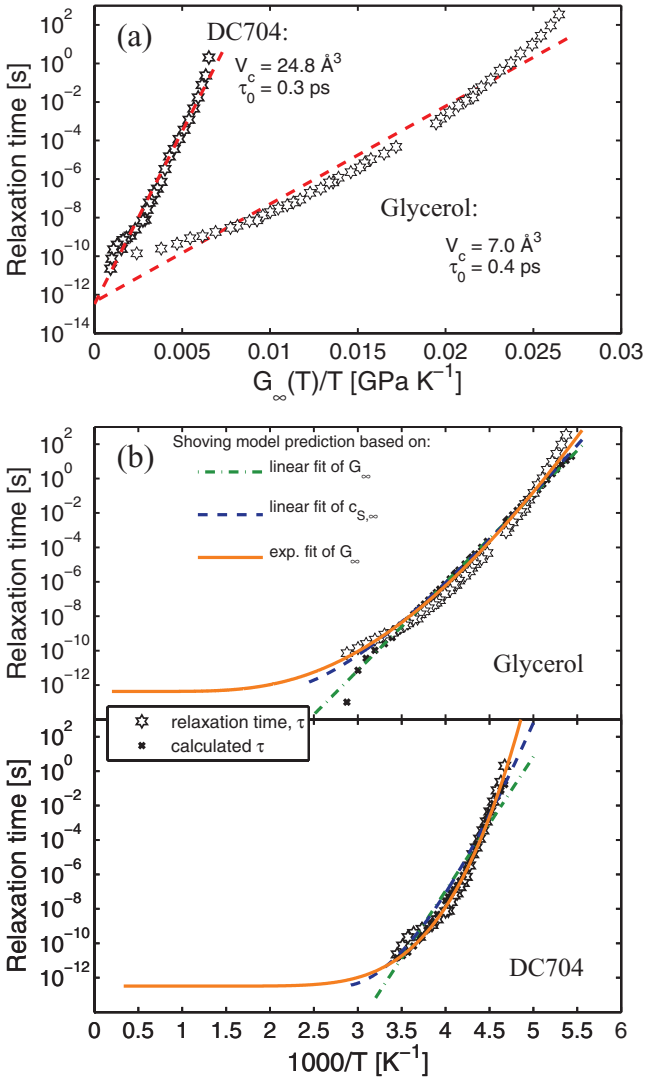

FIG. 9. (a) Relaxation time as a function of inverse temperature scaled by the instantaneous shear modulus, G_∞/T. Assuming the shoving model (Eq. (15)) this plot should linearize the data. In contrast to Figs. 6(c) and 7(c), this plot does refer to a particular glass transition temperature or pre-factor. A linear fit to the data in this plot gives the remaining parameters (V_c and τ_0) of the model. (b) Arrhenius plot of glycerol (top panel) and DC704 (bottom panel). The stars are the relaxation time data plotted as a function of 1000/T. Assuming the shoving model, curves are based on the various fits of $G_\infty(T)$ from Fig. 8 and V_c and τ_0 as determined above. Exponential fit of $G_\infty(T)$: full line, the linear fit of $c_{S,\infty}(T)$: dashed line, the linear fit of $G_\infty(T)$: dashed-dotted line. For glycerol there is little difference between the agreement of the different functional forms of G_∞ and data, probably reflecting the fact that the fits were hardly distinguishable in the region with data. For DC704, on the other hand, the exponential fit (full line) follows almost exactly the data, while the linear fits of G_∞ and c_∞ give poorer agreement.

V. SUMMARY

This paper demonstrated how picosecond ultrasonics can be applied not only to the measurement of longitudinal properties but also to the measurement of shear properties of liquids in the GHz frequency range. For the study of acoustic waves in liquids, our technique of TDBS offers substantial advantages compared with conventional ultrasonic techniques or stimulated scattering techniques (ISS). This is because frequencies (20–100 GHz) much higher than those accessible to the ultrasonic ($\lesssim$100 MHz) or ISS ($\lesssim$1 GHz) techniques, and therefore, instantaneous values of both longitudinal and shear acoustic parameters, i.e., speed of sound, attenuation coefficients and acoustic moduli, can be measured at temperatures significantly higher than T_g. For both liquids, we were able to compile comprehensive dispersion curves that allow for determination of the limiting speeds of sound over large temperature ranges and show the crossover behavior at many different

acoustic frequencies for both longitudinal and shear acoustic waves, although for DC704 there was a discrepancy of ∼10% between the shear speed of sound as inferred from the low-frequency measurements of shear modulus compared to that measured by the high-frequency methods (present results and ISBS results).

We compared our results to data obtained by other spectroscopic techniques. In the case of glycerol, the extracted instantaneous shear modulus allowed us to calculate the shear viscosity, which agrees well with the shear viscosity measured by other means. In both glycerol and DC704, we observe a linear relationship between longitudinal and shear acoustic moduli consistent with a generalized Cauchy relation.

We carried out a shoving model analysis, showing that for both liquids the data are in reasonable agreement with the model, confirming recent findings on other glass-forming liquids.[75–81] For glycerol, the agreement is somewhat poorer than for DC704. One could speculate whether this is correlated with the fact that time-temperature superposition (TTS) is not obeyed by glycerol.[84,85] We do not believe, however, that the sluggishness in the relaxation time introduced by the lack of TTS can account for the deviations.

It should be noted that since V_c of the shoving model (Eq. (15)) represents a finite volume, the use of Eq. (15) implies no divergence of the relaxation time at finite temperatures in agreement with considerations proposed in Ref. 82.

The data indicate that the temperature dependence of the instantaneous shear modulus could be exponential rather than linear. This supports Granato's interstitialcy model.[74]

ACKNOWLEDGMENTS

This work was partially supported by the Department of Energy Grant No. DE-FG02-00ER15087 and National Science Foundation Grant Nos. CHE-0616939 and DMR-0414895. The centre for viscous liquid dynamics "Glass and Time" is sponsored by the Danish National Research Foundation's Grant No. DNRF61.

[1]R. Picarelli and T. A. Litovitz, J. Acoust. Soc. Am. **29**, 1009 (1957).
[2]G. Harrison, *The Dynamic Properties of Supercooled Liquids* (Academic, 1976).
[3]E. Donth, *The Glass Transition* (Springer, Berlin, 2002).
[4]J. C. Dyre, Rev. Mod. Phys. **78**, 953 (2006).
[5]J. C. Dyre, Phys. Rev. E **74**, 021502 (2006).
[6]J. C. Dyre, N. B. Olsen, and T. Christensen, Phys. Rev. B **53**, 2171 (1996).
[7]N. B. Olsen, J. C. Dyre, and T. E. Christensen, Phys. Rev. Lett. **81**, 1031 (1998).
[8]Y. Yan, L. Cheng, and K. A. Nelson, J. Chem. Phys. **88**, 6477 (1988).
[9]S. M. Silence, A. R. Duggal, L. Dhar, and K. A. Nelson, J. Chem. Phys. **96**, 5448 (1992).
[10]Y. Yang and K. A. Nelson, J. Chem. Phys. **103**, 7722 (1995).
[11]Y. Yang and K. A. Nelson, J. Chem. Phys. **103**, 7732 (1995).
[12]D. M. Paolucci and K. A. Nelson, J. Chem. Phys. **112**, 6725 (2000).
[13]D. Pinnow, S. Candau, J. LaMacchia, and T. A. Litovitz, J. Acoust. Soc. Am. **43**, 131 (1968).
[14]A. Giugni and C. A, J. Phys.: Condens. Matter **18**, 889 (2006).
[15]F. Sette, M. H. Krisch, C. Masciovecchio, G. Ruocco, and G. Monaco, Science **280**, 1550 (1998).
[16]C. Thomsen, H. Grahn, H. Maris, and J. Tauc, Phys. Rev. B **34**, 4129 (1986).
[17]O. Matsuda, O. B. Wright, D. H. Hurley, V. E. Gusev, and K. Shimizu, Phys. Rev. Lett. **93**, 095501 (2004).
[18]T. Pezeril, V. Gusev, D. Mounier, N. Chigarev, and P. Ruello, J. Phys. D **38**, 1421 (2005).
[19]C. Rossignol, J. M. Rampnoux, M. Perton, B. Audoin, and S. Dilhaire, Phys. Rev. Lett. **94**, 166106 (2005).
[20]T. Pezeril, N. Chigarev, P. Ruello, D. Mounier, J.-M. Breteau, P. Picart, S. Gougeon, and V. Gusev, Phys. Rev. B **73**, 132301 (2006).
[21]R. N. Kini, A. J. Kent, N. M. Stanton, and M. Henini, Appl. Phys. Lett. **88**, 134112 (2006).
[22]T. Pezeril, P. Ruello, S. Gougeon, N. Chigarev, D. Mounier, J. M. Breteau, P. Picart, and V. Gusev, Phys. Rev. B **75**, 174307 (2007).
[23]T. Pezeril, P. Leon, D. Chateigner, S. Kooi, and K. A. Nelson, Appl. Phys. Lett. **92**, 061908 (2008).
[24]P. Walker, R. P. Campion, A. J. Kent, and C. Jasiukiewicz, Phys. Rev. B **78**, 233307 (2008).
[25]M. Harb, W. Peng, G. Sciaini, C. Hebeisen, R. Ernstofer, M. Eriksson, M. Lagally, S. Kruglik, and R. Miller, Phys. Rev. B **79**, 094301 (2009).
[26]Y.-C. Wen, T.-S. Ko, T.-C. Lu, H.-C. Kuo, J.-I. Chyi, and C.-K. Sun, Phys. Rev. B **80**, 195201 (2009).
[27]V. Gusev, J. Appl. Phys. **107**, 114906 (2010).
[28]M. Msall, O. B. Wright, and A. Matsuda, J. Phys.: Conf. Ser. **92**, 012026 (2007).
[29]T. Pezeril, C. Klieber, S. Andrieu, and K. A. Nelson, Phys. Rev. Lett. **102**, 107402 (2009).
[30]C. Klieber, T. Pezeril, S. Andrieu, and K. A. Nelson, J. Appl. Phys. **112**, 013502 (2012).
[31]J. K. Krüger, J. Balle, T. Britz, A. Le Coutre, R. Peter, R. Bactavatchalou, and J. Schreiber, Phys. Rev. B **66**, 012206 (2002).
[32]C. A. Angell, Science **267**, 1924 (1995).
[33]A. Brodin and E. Rössler, Eur. Phys. J. B **44**, 3 (2005).
[34]K. Niss, B. Jakobsen, and N. B. Olsen, J. Chem. Phys. **123**, 234510 (2005).
[35]K. Schröter and E. Donth, J. Chem. Phys. **113**, 9101 (2000).
[36]R. Slayton and K. A. Nelson, J. Chem. Phys. **120**, 3919 (2004).
[37]J. Wuttke, J. Hernandez, G. Li, G. Coddens, H. Z. Cummins, F. Fujiara, W. Petry, and H. Sillescu, Phys. Rev. Lett. **72**, 3052 (1994).
[38]F. Scarponi, L. Comez, D. Fioretto, and L. Palmieri, Phys. Rev. B **70**, 054203 (2004).
[39]L. Comez, D. Fioretto, F. Scarponi, and G. Monaco, J. Chem. Phys. **119**, 6032 (2003).
[40]C. Glorieux, K. Van de Rostyne, J. Goossens, G. Shkerdin, W. Lauriks, and K. Nelson, J. Appl. Phys. **99**, 013511 (2006).
[41]L. Comez, G. Monaco, C. Masciovecchio, A. Paciaroni, A. Gessini, F. Scarponi, G. Ruocco, and D. Fioretto, Phys. Rev. Lett. **106**, 155701 (2011).
[42]B. Jakobsen, K. Niss, and N. B. Olsen, J. Chem. Phys. **123**, 234511 (2005).
[43]T. Hecksher, N. B. Olsen, K. A. Nelson, J. C. Dyre, and T. Christensen, J. Chem. Phys. **138**, 12A543 (2013).
[44]C. Klieber, E. Peronne, K. Katayama, J. Choi, M. Yamaguchi, T. Pezeril, and K. A. Nelson, Appl. Phys. Lett. **98**, 211908 (2011).
[45]P. Frechard, S. Andrieu, D. Chateigner, M. Hallouis, P. Germi, and M. Pernet, Thin Solid Films **263**, 42 (1995).
[46]A. Devos, M. Foret, S. Ayrinhac, and B. Emery, Phys. Rev. B **77**, 100201 (2008).
[47]S. Ayrinhac, M. Foret, A. Devos, B. Ruffle, E. Courtens, and R. Vacher, Phys. Rev. B **83**, 014204 (2011).
[48]H. N. Lin, R. J. Stoner, H. J. Maris, and J. Tauc, J. Appl. Phys. **69**, 3816 (1991).
[49]K. F. Poulter and P. J. Nash, J. Phys. E **12**, 931 (1979).
[50]I. V. Blazhnov, N. P. Malomuzh, and S. V. Lishchuck, J. Chem. Phys. **121**, 6435 (2004).
[51]R. H. Orcutt, J. Vac. Sci. Technol. **10**, 506 (1973).
[52]P. Lunkenheimer, U. Schneider, R. Brand, and A. Loidl, Contemp. Phys. **41**, 15 (2000).
[53]C. Dreyfus, A. Aouadi, R. M. Pick, T. Berger, A. Patkowski, and W. Steffen, Europhys. Lett. **42**, 55 (1998).
[54]D. H. Torchinsky, J. A. Johnson, and K. A. Nelson, J. Chem. Phys. **136**, 174509 (2012).
[55]B. Jakobsen, T. Hecksher, T. Christensen, N. B. Olsen, J. C. Dyre, and K. Niss, J. Chem. Phys. **136**, 081102 (2012).
[56]U. R. Pedersen, T. Christensen, T. B. Schrøder, and J. C. Dyre, Phys. Rev. E **77**, 011201 (2008).
[57]N. P. Bailey, T. Christensen, B. Jakobsen, K. Niss, N. B. Olsen, U. R. Pedersen, T. B. Schrøder, and J. C. Dyre, J. Phys.: Condens. Matter **20**, 244113 (2008).
[58]N. Gnan, T. B. Schrøder, U. R. Pedersen, N. P. Bailey, and J. C. Dyre, J. Chem. Phys. **131**, 234504 (2009).
[59]C. Klieber, Ph.D. thesis, Massachusetts Institute of Technology (2010), http://dspace.mit.edu/handle/1721.1/57801.

[60]Y. Jeong, S. R. Nagel, and S. Bhattacharya, Phys. Rev. A **34**, 602 (1986).
[61]Y. H. Jeong, Phys. Rev. A **36**, 766 (1987).
[62]D. H. Torchinsky, T. Hecksher, C. Klieber, J. A. Johnson, J. C. Dyre, and K. A. Nelson "Ultra broadband mechanical spectroscopy of the glass-forming material DC704" (unpublished).
[63]Y.-X. Yan and K. A. Nelson, J. Chem. Phys. **87**, 6240 (1987).
[64]Y.-X. Yan and K. A. Nelson, J. Chem. Phys. **87**, 6257 (1987).
[65]M. Born and K. Huang, *Dynamical Theory of Crystal Lattices* (Oxford University Press, 1954).
[66]J. K. Krüger, U. Müller, R. Bactavatchalou, J. Mainka, C. Gilow, W. Possart, A. Tschöpe, P. Alnot, D. Rouxel, R. Sanctuary, and B. Wetzel, J. Phys. IV **129**, 45 (2005).
[67]P. Wen, J. P. Johari, R. J. Wang, and W. H. Wang, Phys. Rev. B **73**, 224203 (2006).
[68]J. C. Dyre, J. Non-Cryst. Solids **235–237**, 142 (1998).
[69]R. W. Hall and P. G. Wolynes, J. Chem. Phys. **86**, 2943 (1987).
[70]J. C. Dyre, Phys. Rev. Lett. **58**, 792 (1987).
[71]J. C. Dyre and N. B. Olsen, Phys. Rev. E **69**, 042501 (2004).
[72]T. B. Schrøder, S. Sastry, J. Dyre, and S. C. Glotzer, J. Chem. Phys. **112**, 9834 (2000).
[73]A. V. Granato, Phys. Rev. Lett. **68**, 974 (1992).
[74]A. V. Granato, J. Non-Cryst. Solids **357**, 334 (2011).
[75]C. Maggi, B. Jakobsen, T. Christensen, N. B. Olsen, and J. C. Dyre, J. Phys. Chem. B **112**, 16320 (2008).
[76]D. H. Torchinsky, J. A. Johnson, and K. A. Nelson, J. Chem. Phys. **130**, 064502 (2009).
[77]V. A. Khonik, Y. P. Mitrofanov, S. A. Lyakhov, A. N. Vasiliev, S. V. Khonik, and D. A. Khoviv, Phys. Rev. B **79**, 132204 (2009).
[78]B. Xu and G. B. McKenna, J. Chem. Phys. **134**, 124902 (2011).
[79]T. Rouxel, J. Chem. Phys. **135**, 184501 (2011).
[80]W. Wang, J. Appl. Phys. **110**, 053521 (2011).
[81]M. C. C. Ribeiro, J. Non-Cryst. Sol. **355**, 1659 (2009).
[82]T. Hecksher, A. I. Nielsen, N. B. Olsen, and J. C. Dyre, Nat. Phys. **4**, 737 (2008).
[83]G. Monaco, D. Fioretto, L. Comez, and G. Ruocco, Phys. Rev. E **63**, 061502 (2001).
[84]N. B. Olsen, T. Christensen, and J. C. Dyre, Phys. Rev. Lett. **86**, 1271 (2001).
[85]F. Kremer and A. Schönhals, *Broadband Dielectric Spectroscopy* (Springer-Verlag, Berlin/Heidelberg, 2003).